

A Nearly Polar Orbit for the Extrasolar Hot Jupiter WASP-79b¹

B. C. Addison^{1,2}, C. G. Tinney^{1,2}, D. J. Wright^{1,2}, D. Bayliss³, G. Zhou³, J. D. Hartman^{4,5},
G. Á Bakos^{4,5}, and B. Schmidt³
b.addison@unsw.edu.au

ABSTRACT

We report the measurement of a spin-orbit misalignment for WASP-79b, a recently discovered, extremely bloated transiting hot Jupiter from the WASP survey. Data were obtained using the CYCLOPS2 optical-fiber bundle and its simultaneous calibration system feeding the UCLES spectrograph on the Anglo-Australian Telescope at the Siding Spring Observatory. We have used the Rossiter-McLaughlin effect to determine the sky-projected spin-orbit angle to be $\lambda = -106^{+10}_{-8}^\circ$. This result indicates a significant misalignment between the spin axis of the host star and the orbital plane of the planet – the planet being in a nearly polar orbit. WASP-79 is consistent with other stars that have $T_{eff} > 6250\text{K}$ and host hot Jupiters in spin-orbit misalignment.

Subject headings: planets and satellites: dynamical evolution and stability — stars: individual (WASP-79) — techniques: radial velocities

1. INTRODUCTION

Over 800 extrasolar planets² have been discovered by various methods in the past two decades, strengthening our understanding of planetary formation and migration. Radial velocity searches, utilizing the Doppler shift of spectral absorption lines due to the orbital motion of a planet, have historically been the most fruitful technique for finding planets (Bottom et al. 2013). In re-

cent years, ground based transit surveys such as WASP (Pollacco et al. 2006), HAT-Net (Bakos et al. 2004), and HATSouth (Bakos et al. 2013) and space based transit surveys like Kepler (Borucki et al. 2010), which measure the decrease in flux of the host star due to the planet moving in front of it, have been leading the charge in discovering a host of new planets (Batalha et al. 2013).

With so many planets now discovered, the focus has shifted more towards understanding their structure, composition, and other bulk properties so as to provide insights into the processes involved in planetary formation, evolution and migration (Santos 2008). One example of this is the combination of transit and radial velocity data for transiting planets which provides a direct measurement of their masses (from radial velocity observations) and radii (from transit observations), and hence their bulk densities – a critical physical measurement needed for the characterization of exoplanets (Mordasini et al. 2012).

An additional probe of planetary formation and migration is provided by accurately measuring the sky-projected spin-orbit alignment (or obliquity) through spectroscopic measurements of the

¹Exoplanetary Science Group, School of Physics, University of New South Wales, 2052, Australia

²Australian Centre of Astrobiology, University of New South Wales, 2052, Australia

³Research School of Astronomy and Astrophysics, Australian National University, Canberra, ACT 2611, Australia

⁴Department of Astrophysical Sciences, Princeton University, NJ 08544, USA

⁵Harvard-Smithsonian Center for Astrophysics, Cambridge, MA 02138, USA

¹Based on observations obtained at the Anglo-Australian Telescope, Siding Spring, Australia.

²exoplanet.eu, as of 2013 May. For “discovery” we adopt the requirement that a transit is both detected and confirmed by Doppler observations, and so do not include the several thousand planet candidates published by Kepler.

Rossiter-McLaughlin effect (Winn et al. 2005). This effect is caused by the modification of the stellar spectrum produced as a transiting planet occults a small region of the stellar disk of its host star, causing asymmetric distortions in the stellar line profiles that result in a radial velocity anomaly (see e.g. Rossiter 1924; McLaughlin 1924; Ohta et al. 2005).

This effect for planets was first observed by Queloz et al. (2000) for HD209458b and is being detected for a growing number of planetary systems (see e.g. Albrecht et al. 2012b). Planets are expected to form in the proto-stellar/proto-planetary disk that surrounds a protostar (e.g. Pollack et al. 1996). The dominant core-accretion paradigm for this formation process predicts that the stellar spin and planetary orbital axes should generally be aligned (e.g. Ohta et al. 2005; Winn et al. 2005) – as in the case of our own solar system which is in alignment to within 6° (Beck and Giles 2005). However, the large number of inward migrated Jovian exoplanets (also known as hot Jupiters) with orbital periods of only a few days seems to suggest that many exoplanetary systems have had a more complex formation history than the Solar System. Various planetary migration mechanisms – including planet-planet scattering (Weidenschilling and Marzari 1996), Kozai resonances (Kozai 1962; Naoz et al. 2011), tidal friction, or some combination of these processes (e.g. Nagasawa et al. 2008; Naoz et al. 2012; Hartman et al. 2012) – have been proposed to explain misaligned systems though none have robustly predicted the misalignment of all observed systems.

In this letter, we present spectroscopic follow-up measurements obtained during the transit of WASP-79b, a recently discovered hot Jupiter from the WASP Southern Hemisphere transit survey (Smalley et al. 2012). WASP-79b has a mass M_P of $0.90 \pm 0.09 M_J$, radius R_P of $1.70 \pm 0.11 R_J$, and orbits an F5 star with $T_{eff} = 6600 \pm 100\text{K}$ (Smalley et al. 2012). We detect a clear radial velocity anomaly due to the Rossiter-McLaughlin effect and from these measurements determine that this system is significantly misaligned and lies in a nearly polar orbit.

2. OBSERVATIONS

We obtained high-precision radial velocity observations of WASP-79 using the CYCLOPS³ optical-fiber bundle feeding the UCLES echelle spectrograph on the 3.9m Anglo-Australian Telescope at Siding Spring Observatory, Australia. CYCLOPS2 is a Cassegrain fiber-based integral field unit which reformats a $\sim 2.5''$ diameter aperture into an equivalent slit of dimensions $0.6''$ wide and $14.5''$ long (Horton et al. 2012). It has replaced an earlier incarnation (CYCLOPS CLASSIC)⁴ which had 15 fibers (of which 3 were inoperative) and 10% lower throughput. CYCLOPS2 has 16 functioning on-sky fibers, plus one fiber for the simultaneous ThXe arc calibrations for every exposure. Each fiber delivers a spectral resolution of $\lambda/\Delta\lambda \approx 70,000$ over 19 echelle orders in the wavelength range of 4550–7350 Å, when used with the UCLES spectrograph in its 79 line/mm grating configuration.

WASP-79 was observed continuously on the night of 2012 December 23, starting $\sim 20\text{min}$ before transit ingress and finishing $\sim 2\text{h}$ after egress. A total of 23 spectra were taken with 800s exposures and readout times of 120s for a cadence of 920s over a period of nearly 7h, with 14 exposures lying in the $\sim 3.8\text{h}$ transit duration. The overall observing conditions were very good with seeing ranging from $0.9''$ to $1.2''$ and mostly clear skies. The airmass at which WASP-79 was observed varied between 1.1 at the start of the night to ~ 1.0 near mid transit and 1.7 at the end of the night. For these observations, the simultaneous ThXe wavelength calibration system delivers two significant advantages. First, it eliminates the need for object observations to be bracketed by arc wavelength calibrations thus providing an additional 240s on-sky per object exposure. Secondly, the error in the wavelength solution from the interpolation of two bracketed arc exposures is eliminated because the wavelength solution is obtained from the ThXe taken simultaneously with each object exposure.

The data was reduced using custom MATLAB routines developed by the authors. These use a wavelength solution computed from a reference

³http://www.phys.unsw.edu.au/~cgt/CYCLOPS/CYCLOPS_2.html

⁴http://www.phys.unsw.edu.au/~cgt/CYCLOPS/CYCLOPS_Classic.html

ThAr image that was then distorted to account for differences between the reference ThAr arc, and the ThXe calibrations obtained from each stellar image (Wright and Tinney, in prep.). Radial velocities for each of the 16 individual fibers in each of the 18 orders for WASP-79 were calculated using the IRAF⁵ task, *fxcor*, by cross-correlation with a spectrum of a bright template star (HD86264) of similar spectral type. HD86264 was observed on the same night as WASP-79 at an airmass of ~ 1.1 , with a 1200s exposure, and a S/N= 115 (2.5 pixels per resolution element) at $\lambda = 5490\text{\AA}$. *Fxcor* implements the standard cross-correlation technique developed by Tonry and Davis (1979). Fitted Gaussians encompassing $\sim 80\%$ of the peak in the cross-correlation function were used to compute each of the radial velocities and their associated uncertainties. We experimented with a variety of templates for cross-correlation including the highest signal-to-noise observation of WASP-79 and a synthetic spectrum, however, we found that the lowest inter-fiber and inter-order velocity scatter was obtained using the spectrum of HD86264. Weighted radial velocities for each observation were determined by first clipping velocities from fibers with Tonry & Davis R numbers less than 10. The R number is the ratio height between the true peak and that of the average peak in the Gaussian fit to the cross-correlation function (Tonry and Davis 1979). We found that the radial velocities with an associated $R < 10$ were unreliable as the peak in cross-correlation function was not very Gaussian shaped (thus could not be well fit) and not significantly above the noise in the rest of the cross-correlation function. After R clipping, a further 3σ clip was performed on the remaining velocities, from which a weighted mean was computed. Uncertainties for each of the weighted radial velocities were estimated from the weighted standard deviation of the velocity scatter of all the fibers over all the orders used.

⁵IRAF is distributed by the National Optical Astronomy Observatories, which are operated by the Association of Universities for Research in Astronomy, Inc., under cooperative agreement with the National Science Foundation.

3. ANALYSIS

To determine the magnitude of the Rossiter-McLaughlin effect and accurately measure the spin-orbit alignment, we have developed a model we call the Exoplanetary Orbital Simulation and Analysis Model (ExOSAM). This model simulates the orbital position of a planet at the time of each observation using standard planetary orbital mechanics equations (Prussing and Conway 2012). From this, ExOSAM computes the velocity from the motion of the star due to the orbiting planet and the in-transit lightcurve including the velocity anomaly due to the Rossiter-McLaughlin effect.

There are 13 parameters used by ExOSAM to compute the best fit model for the Rossiter-McLaughlin anomaly: two are initially free (the projected spin-orbit angle, λ , and projected stellar rotational velocity, $(v \sin i)_*$); and 11 are fixed (planet-to-star mass ratio (M_p/M_*), planet-to-star radius ratio (R_p/R_*), the orbital inclination angle (i), orbital eccentricity (e), the adopted linear limb-darkening coefficient (μ), the micro-turbulence velocity (ξ_t), the macro-turbulence velocity (v_{mac}), the orbital period (P), the center-of-mass velocity (V_{TP}) at published epoch T_P , the mid transit time (T_0) at the epoch of observation, and the radial velocity offset (V_d) between the published epoch T_P and the epoch we observed at T_0). This last parameter is fixed in the Rossiter-McLaughlin fit, but determined from the two data sets outside the transit event. The remaining fixed parameters were adopted from Smalley et al. (2012) and their values and uncertainties are listed in Table 1.

The best-fitting values for λ and $(v \sin i)_*$ are derived using a grid search and minimizing χ^2 between the observed radial velocities and modeled radial velocities. Initial estimates for λ and $(v \sin i)_*$ were derived by visual inspection and on a grid with intervals of 0.5° in λ and 50 ms^{-1} in $(v \sin i)_*$ that was searched in the range -60° to -140° and 12000 ms^{-1} to 24000 ms^{-1} respectively. The 1σ confidence levels for these parameters were determined through the $\Delta\chi^2$ method (Bradt 2004) which is based on the probability distribution of χ^2 as a function of the confidence level and degrees of freedom.

Various approaches for modeling the velocity anomaly ($\Delta v(t)$) caused by a planet as a func-

tion of its orbital parameters are available, including the first-moment approach (Ohta et al. 2005), stellar absorption line profile modeling approach (Hirano et al. 2011), and the forward-modeling approach (Winn et al. 2005). In our case, the most applicable and straight forward approach is to implement the Hirano et al. (2010) analytic solution given in Equation (1). It has been used in many studies (for example Bayliss et al. 2010) and was also independently derived by Boué et al. (2013) specifically for the cross-correlation method of computing velocities.

$$\Delta v(t) = -f(t)v_p(t) \left[\frac{2v_0^2 + 2(v \sin i)_*^2}{2v_0^2 + (v \sin i)_*^2} \right]^{3/2} \left[1 - \frac{v_p(t)^2}{2v_0^2 + (v \sin i)_*^2} \right] \quad (1)$$

The velocity anomaly as a function of time due to the Rossiter-McLaughlin effect is $\Delta v(t)$, $f(t)$ is the flux and $v_p(t)$ is the “sub-planet” or line-of-sight velocity of the occulted region as a function of time respectively, $(v \sin i)_*$ is the projected stellar rotational velocity, and v_0 is the velocity width of the spectral lines from the occulted region due to mechanisms other than stellar rotation such as micro-turbulence and/or macro-turbulence.

The flux $f(t)$ is calculated by assuming a linear limb-darkening law for the stellar surface using the analytic equation given by Diaz-Cordoves et al. (1995) and fixing an interpolated limb-darkening coefficient from look-up tables given in Diaz-Cordoves et al. (1995) based on the assumed stellar parameters of WASP-79 from Smalley et al. (2012). The sub-planet velocity $v_p(t)$ is calculated assuming that the rotation of the star is uniform (i.e. that it is not differentially rotating) with the angle λ between the sky projected stellar spin axis and the planetary orbital angular momentum vector (Winn et al. 2005). The projected stellar rotational velocity $(v \sin i)_*$ is a free parameter in our model.

The overall best fit parameters including their uncertainties and estimated S/N (2.5 pixel per resolution element) are given in Table 1. Smalley et al. (2012) were unable to uniquely determine the radius of WASP-79, and derived two preferred solutions – one with WASP-79 on the main sequence ($R_* = 1.64 \pm 0.08 R_\odot$) and one with it evolved just off the main sequence ($R_* = 1.91 \pm 0.09 R_\odot$). They concluded that the main sequence solution is the more likely one, nonetheless, we have performed our fit with both the main sequence and non-main sequence parameters for WASP-79. Table 2 in-

cludes our weighted radial velocities at each epoch. Figure 1 shows the modeled velocity anomaly for the preferred main sequence solution with the observed velocities over-plotted. The filled in blue circles with red error bars are velocities we measured, while the black open circles overlaid with an x and with blue error bars are previously published velocities in Smalley et al. (2012). The $\lambda - (v \sin i)_*$ probability space for the main sequence solution is shown in Figure 2.

Our results for the projected spin-orbit alignment and stellar rotation velocity, using the main sequence parameters, are $\lambda = -106_{-8}^{+10}^\circ$ and $(v \sin i)_* = 17.5_{-1.4}^{+1.3} \text{ kms}^{-1}$. For the non-main sequence case, $\lambda = -85_{-33}^{+13}^\circ$ and $(v \sin i)_* = 16.0_{-1.3}^{+1.3} \text{ kms}^{-1}$. We obtain a considerably worse fit from the non-main sequence solution. Additionally, the uncertainty on λ is much larger. Thus we conclude that WASP-79 is more likely to be a main sequence star, however, we caution the reader that our measurement of the Rossiter-McLaughlin effect alone cannot constrain this systems parameters. High precision transit photometry is required in order to nail down this systems parameters.

For the main sequence case of WASP-79, the $(v \sin i)_*$ value we measured is consistent (within uncertainties) with Smalley et al. (2012) published value of $(v \sin i)_* = 19.1 \pm 0.7 \text{ kms}^{-1}$. As a further check of this value, we independently measured $(v \sin i)_*$ using the highest signal-to-noise spectrum of WASP-79. This was done by fitting a rotationally broadened Gaussian (Gray 2005) to a least-squares deconvolution profile (Donati et al. 1997) obtained for each spectral order of WASP-79. The distribution of values along with an examination of the goodness of the fits was used to estimate the uncertainty for this $(v \sin i)_*$ measurement (Gray 2005). This results in a value of $(v \sin i)_* = 18.2 \pm 0.2 \text{ kms}^{-1}$ – again consistent with (Smalley et al. 2012) and the Rossiter-McLaughlin measurements.

The Rossiter-McLaughlin effect is clearly detected as a positive “hump-shaped” anomaly (see Figure 1). The planet transits across only the blue-shifted hemisphere (i.e. the side rotating towards us) during the transit event and thus the star appears to be anomalously red-shifted. Based on the shape of the velocity anomaly, WASP-79b

appears to be nearly in a polar orbit. This system is part of only a handful of planetary systems in near-polar⁶ (9 out of 70 systems with spin-orbits measured)⁷ and/or retrograde⁶ orbits (7 out of 70 systems with spin-orbits measured)⁷. For examples of such systems see WASP-7b (Albrecht et al. 2012a), CoRoT-1b (Pont et al. 2010), HAT-P-11b (Winn et al. 2010b), HAT-P-32b (Albrecht et al. 2012b), WASP-1b (Simpson et al. 2011), and WASP-80b (Triaud et al. 2013).

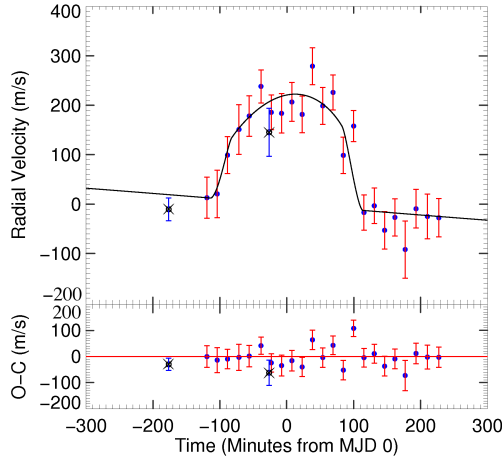


Fig. 1.— Spectroscopic radial velocities of the WASP-79b transit. Velocity from just before, during, and after the transit are plotted as a function of time along with the best fitting model (for the main-sequence parameters) and corresponding residuals. The filled in blue circles with red error bars are velocities we measured with our estimated uncertainty. The two black open circles overlaid with an x and with blue error bars are previously published velocities by Smalley et al. (2012) using their quoted uncertainties.

4. DISCUSSION

As of April 2013, 70 exoplanetary systems have measured spin-orbit alignments. Of these, twenty-

⁶We have adopted near-polar orbits as those with spin-orbit angles between $\frac{3\pi}{8} < \lambda < \frac{5\pi}{8}$ or $\frac{-3\pi}{8} > \lambda > \frac{-5\pi}{8}$ and retrograde orbits for spin-orbit angles between $\frac{5\pi}{8} \leq \lambda \leq \frac{11\pi}{8}$ or $\frac{-5\pi}{8} \geq \lambda \geq \frac{-11\pi}{8}$.

⁷This study has made use of René Heller's Holt-Rossiter-McLaughlin Encyclopaedia and was last updated on 2013 May. http://ooo.aip.de/People/rheller/content/main_spinorbit.html

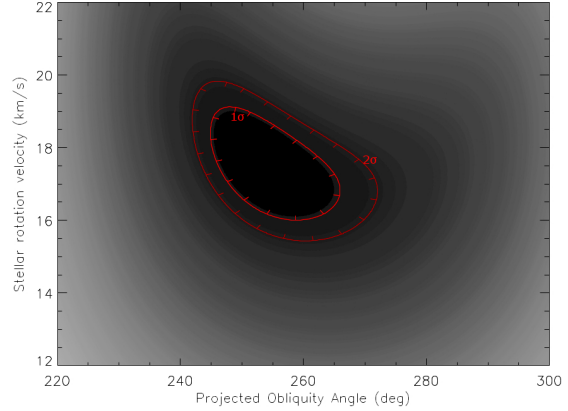


Fig. 2.— Contours marking the $\lambda - (v \sin i)_*$ probability space are shown for the main sequence parameters of WASP-79. The 1 and 2σ uncertainties from the fitted parameters are shown.

Table 1: System parameters for WASP-79

Parameter	Value (ms)	Value (no-ms)
<i>Parameters as given by Smalley et al. (2012) and used as priors in model</i>		
Mid-transit epoch (2400000-HJD), T_0	56285.03459 ± 0.00200	56285.03739 ± 0.00300
Orbital period, P	3.6623817 ± 0.0000050 d	3.6623866 ± 0.0000085 d
Orbital inclination, i	$85.4 \pm 0.6^\circ$	$83.3 \pm 0.5^\circ$
Orbital eccentricity, e	0.0	0.0
Stellar mass, M_*	$1.56 \pm 0.09 M_\odot$	$1.52 \pm 0.07 M_\odot$
Stellar radius, R_*	$1.64 \pm 0.08 R_\odot$	$1.91 \pm 0.09 R_\odot$
Planet mass, M_p	$0.90 \pm 0.09 M_J$	$0.90 \pm 0.08 M_J$
Planet radius, R_p	$1.70 \pm 0.11 R_J$	$2.09 \pm 0.14 R_J$
Stellar micro-turbulence, ξ_t	1.3 ± 0.1	$1.3 \pm 0.1 \text{ km s}^{-1}$
Stellar macro-turbulence, v_{mac}	$6.4 \pm 0.3 \text{ km s}^{-1}$	$6.4 \pm 0.3 \text{ km s}^{-1}$
Stellar limb-darkening coefficient, μ	0.606 (adopted)	0.606 (adopted)
Velocity at published epoch T_p , V_{Tp}	$4.9875 \pm 0.0004 \text{ km s}^{-1}$	$4.9875 \pm 0.0004 \text{ km s}^{-1}$
RV offset, V_d	0.2575 km s^{-1}	0.2575 km s^{-1}
<i>Parameters determined from model fit using our velocities</i>		
Projected obliquity angle, λ	$-106^{+10}_{-8}^\circ$	$-85^{+12}_{-3}^\circ$
Projected stellar rotation velocity, $(v \sin i)_*$	$17.5^{+1.3}_{-1.4} \text{ km s}^{-1}$	$16.0^{+1.3}_{-1.3} \text{ km s}^{-1}$
<i>Independent measurement of $(v \sin i)_{*(ind)}$ and Smalley et al. (2012) $(v \sin i)_{*(S)}$ published value</i>		
Projected stellar rotation velocity, $(v \sin i)_{*(ind)}$	$18.2 \pm 0.2 \text{ km s}^{-1}$	$18.2 \pm 0.2 \text{ km s}^{-1}$
Projected stellar rotation velocity, $(v \sin i)_{*(S)}$	$19.1 \pm 0.7 \text{ km s}^{-1}$	$19.1 \pm 0.7 \text{ km s}^{-1}$

nine⁷ show substantial misalignments ($\lambda > \frac{\pi}{8} = 22.5^\circ$), nine are nearly polar orbits⁷, and seven⁷ are in retrograde orbits. With such a significant fraction of planets in spin-orbit misalignment, there is a clear need to understand the physical mechanisms that generates such high occurrence rates. Several mechanisms have been proposed based on apparent trends in planetary orbital obliquity. One such trend noted by Winn et al. (2010a) is that hot stars with $T_{eff} > 6250$ K tend to host planets which are in spin-orbit misalignment. Winn et al. (2010a) suggest that this can be understood if the convective layer in hot stars is too thin to effectively align the planet's orbital plane while cool stars have a thicker convective layer thus dampening orbital obliquities towards alignment in short time-scales.

This conclusion has more recently been supported by the work of Albrecht et al. (2012b). After measuring the Rossiter-McLaughlin effect for 14 new systems and including the 39 previously published systems (at the time of their publication) in their analysis, they found a positive correlation between obliquity and stellar temperature (higher obliquity orbits around hotter stars), an inverse correlation for stellar age (orbits are more aligned around older stars), and a positive correlation for tidal dissipation timescales (higher obliquity orbits around stars with longer tidal dissipation timescales). They reason that hotter, more massive stars tend to have a thinner convective envelope as supported by stellar interior models (Pinsonneault et al. 2001), and that it is the convection envelope that is responsible for dampening the tidal energy and driving planets into alignment. This suggest that hotter stars are more likely to host planets in spin-orbit misalignment. They conclude by suggesting that the various mechanisms which caused Jupiter mass planets to migrate inwards in the first place also produced randomly distributed orbital obliquities (it is likely that hot Jupiters initially formed with low obliquity orbits as predicted by the core-accretion model as suggested by Ohta et al. (2005) and Winn et al. (2005)). After migration, systems with short tidal dampening timescales and strong tidal interactions quickly align their planets, while systems with longer tidal dampening timescales and/or weak tidal interactions will still display more random obliquity distributions long after migration.

Does WASP-79b align with the model of Albrecht et al. (2012b)? WASP-79 has an effective temperature of $T_{eff} = 6600 \pm 100\text{K}$, which

is above the $T_{eff} > 6250\text{K}$ threshold claimed for planetary systems displaying more randomly distributed obliquities. Using either of the two methods presented by Albrecht et al., the tidal dissipation timescale for WASP-79 is found to be very long – somewhere in the range $\tau_{mcz} = 1.6 \times 10^{11}\text{yr}$ to $\tau_{RA} = 3.3 \times 10^{15}\text{yr}$ (for an assumed main sequence age of WASP-79 between 0.5 and 3.5 Gyr). WASP-79, then, has a tidal dissipation timescale longer than 95% of the systems examined by Albrecht et al., making it consistent with the observed trend of finding planets in high obliquity orbits in systems with long tidal-dampening timescales.

5. CONCLUSION

WASP-79b is in an orbit that is significantly misaligned with the projected rotational axis of its host star either by $\lambda = -106_{-8}^{+10}^\circ$ (main sequence parameters) or $\lambda = -85_{-33}^{+13}^\circ$ (non-main sequence parameters). This places the planet in a near-polar orbit. Conventional planetary formation models, such as core-accretion, do not predict Jovian type planets orbiting within 0.1AU from their host star to be in highly misaligned orbits (Ohta et al. 2005; Winn et al. 2005). Yet the WASP-79 planetary system joins a growing list of known systems that are in significant spin-orbit misalignment (as shown in the study by Albrecht et al. 2012b). Additionally, planets that are thought to have undergone migration primarily due to the traditional Type 1 and Type 2 migration mechanisms (Lin et al. 1996) are predicted not to have their orbits significantly misaligned (Bate et al. 2010).

A variety of mechanisms have been proposed to explain these systems (see for example Weiden-schilling and Marzari 1996; Kozai 1962; Naoz et al. 2011). However, it is only within the last year has there been a large enough sample of measured obliquities to begin looking for correlations and testing these mechanisms. Nonetheless, further expansion of the sample of planetary systems from which we can measure spin-orbit angles is needed to understand the mechanisms driving planetary migration and observed spin-orbit misalignments. Globally distributed ground-based transit searches such as HATSouth (Bakos et al. 2013) and new space based all-sky transit survey TESS (Deming

Table 2: Radial Velocities for WASP-79 (fiber and order averaged) with one previously published velocity during transit.

Time	RV	S/N at	Time	RV	S/N at
BJD-2400000	$\pm\sigma_{RV}(\text{ms}^{-1})$	$\lambda=5490\text{\AA}$	BJD-2400000	$\pm\sigma_{RV}(\text{ms}^{-1})$	$\lambda=5490\text{\AA}$
55874.83089 ^a	5133 ± 49^a	N/A ^a	56285.07329	4929 ± 37	29
56284.95307	4743 ± 42	35	56285.08398	4956 ± 36	30
56284.96377	4751 ± 48	35	56285.09467	4829 ± 37	32
56284.97446	4829 ± 38	37	56285.10537	4888 ± 31	35
56284.98633	4881 ± 50	35	56285.11606	4713 ± 36	37
56284.99701	4909 ± 41	35	56285.12675	4727 ± 36	35
56285.00914	4969 ± 33	37	56285.13745	4677 ± 38	30
56285.01984	4916 ± 35	37	56285.14814	4703 ± 38	29
56285.03052	4914 ± 40	37	56285.15884	4638 ± 58	24
56285.04122	4937 ± 39	29	56285.17011	4721 ± 39	27
56285.05191	4912 ± 37	27	56285.18196	4705 ± 45	22
56285.06260	5009 ± 37	29	56285.19381	4703 ± 39	24

^a Published radial velocity by Smalley et al. (2012) during transit.

et al. 2009) are set to deliver such samples before the decade is out, setting the scene for spin-orbit alignment measurements to play a key role in elucidating the complex formation and orbital evolution mechanisms of extra-solar planets.

The research work presented in the paper at UNSW has been supported by ARC Australian Professorial Fellowship grant DP0774000, ARC LIEF grant LE0989347 and ARC Super Science Fellowships FS100100046. Work at the Australian National University is supported by ARC Laureate Fellowship Grant FL0992131. We acknowledge the use of the SIMBAD database, operated at CDS, Strasbourg, France.

REFERENCES

- Albrecht, S., Winn, J. N., Butler, R. P., et al. 2012a, *ApJ*, 744, 189
- Albrecht, S., Winn, J. N., Johnson, J. A., et al. 2012b, *ApJ*, 757, 18
- Bakos, G. Á., Noyes, R. W., Kovács, G., et al. 2004, *PASP*, 116, 266
- Bakos, G. Á., Csubry, Z., Penev, K., et al. 2013, *PASP*, 125, 154
- Batalha, N. M., Rowe, J. F., Bryson, S. T., et al. 2013, *ApJS*, 204, 24
- Bate, M. R., Lodato, G., & Pringle, J. E. 2010, *MNRAS*, 401, 1505
- Bayliss, D. D. R., Winn, J. N., Mardling, R. A., et al. 2010, *ApJ*, 722, L224
- Beck, J. G. & Giles, P. 2005, *ApJ*, 621, L153
- Borucki, W. J., Koch, D., Basri, G., et al. 2010, *Science*, 327, 977
- Bottom, M., Muirhead, P. S., Asher Johnson, J., et al. 2013, *PASP*, 125, 240
- Boué, G., Montalto, M., Boisse, I., et al. 2013, *A&A*, 550, A53
- Bradt, H. 2004, *Cambridge Planetary Science*
- Deming, D., Seager, S., Winn, J., et al. 2009, *PASP*, 121, 952
- Diaz-Cordoves, J., Claret, A., & Gimenez, A. 1995, *A&AS*, 110, 329
- Donati, J. -F., et al. 1997, *MNRAS*, 291, 658
- Gray, D. F. 2005, *Cambridge*
- Hartman, J. D., Bakos, G. Á., Béky, B., et al. 2012, *AJ*, 144, 139
- Hirano, T., Suto, Y., Taruya, A., et al. 2010, *ApJ*, 709, 458
- Hirano, T., Suto, Y., Winn, J. N., et al. 2011, *ApJ*, 742, 69
- Horton, A., Tinney, C. G., Case, S., et al. 2012, In *Society of Photo-Optical Instrumentation Engineers (SPIE) Conference Series*, Vol. 8446, Society of Photo-Optical Instrumentation Engineers (SPIE) Conference Series
- Kozai, Y. 1962, *AJ*, 67, 591
- Lin, D. N. C., Bodenheimer, P., & Richardson, D. C. 1996, *Nature*, 380, 606
- McLaughlin, D. B. 1924, *ApJ*, 60, 22
- Mordasini, C., Alibert, Y., Klahr, H., et al. 2012, *A&A*, 547, A111
- Nagasawa, M., Ida, S., & Bessho, T. 2008, *ApJ*, 678, 498
- Naoz, S., Farr, W. M., Lithwick, Y., et al. 2011, *Nature*, 473, 187
- Naoz, S., Farr, W. M., & Rasio, F. A. 2012, *ApJ*, 754, L36
- Ohta, Y., Taruya, A., & Suto, Y. 2005, *ApJ*, 622, 1118
- Pinsonneault, M. H., DePoy, D. L., & Coffee, M. 2001, *ApJ*, 556, L59
- Pollacco, D. L., Skillen, I., Collier Cameron, A., et al. 2006, *PASP*, 118, 1407
- Pollack, J. B., Hubickyj, O., Bodenheimer, P., et al. 1996, *Icarus*, 124, 62
- Pont, F., Endl, M., Cochran, W. D., et al. 2010, *MNRAS*, 402, L1
- Prussing, J. & Conway, B. 2012, *Oxford University Press*
- Queloz, D., Eggenberger, A., Mayor, M., et al. 2000, *A&A*, 359, L13
- Rossiter, R. A. 1924, *ApJ*, 60, 15
- Santos, N. C. 2008, *New A Rev.*, 52, 154
- Simpson, E. K., Pollacco, D., Cameron, A. C., et al. 2011, *MNRAS*, 414, 3023
- Smalley, B., Anderson, D. R., Collier-Cameron, A., et al. 2012, *A&A*, 547, A61
- Tonry, J. & Davis, M. 1979, *AJ*, 84, 1511
- TriAUD, A. H. M. J., Anderson, D. R., Collier Cameron, A., et al. 2013, *A&A*, 551, A80
- Weidenschilling, S. J. & Marzari, F. 1996, *Nature*, 384, 619
- Winn, J. N., Fabrycky, D., Albrecht, S., et al. 2010a, *ApJ*, 718, L145
- Winn, J. N., Johnson, J. A., Howard, A. W., et al. 2010b, *ApJ*, 723, L223
- Winn, J. N., Noyes, R. W., Holman, M. J., et al. 2005, *ApJ*, 631, 1215